ACTA IMEKO
ISSN: 2221-870X
March 2026, Volume 15, Number 1, 1 - 8

Development of a real-time 3D camera based on micro-electromechanical systems mirrors

Paolo Diotti[1,2], Daniele Caltabiano[1], Anna Angela Pomarico[1], Giuditta Roselli[1], Michele Norgia[2]

[1] *STMicroelectronics s.r.l., Agrate Brianza, Italy*
[2] *Politecnico di Milano, 20134 Milan, Italy*

ABSTRACT
In this study, we describe the realization of a time-of-flight scanning LiDAR (Light Detection and Ranging) prototype, that leverages mirrors as micro-electromechanical systems (MEMS) for agile beam steering in a compact size, and a field-programmable gate array (FPGA)-based processing unit for real-time 3D image reconstruction. The proposed 3D LiDAR system is designed to operate within a range of up to 1 meter with a spatial resolution of 400 × 300 pixels at a frame rate of 30 Hz. The LiDAR prototype architecture consists of 3 main parts: an optomechanical system, a digital processing unit (FPGA-based), an analog front-end. Processed 3D depth maps are rendered in real time via a high-definition multimedia interface (HDMI), providing immediate visual feedback. The full system was deeply characterized and tested. The integration of MEMS mirrors, an FPGA-based time-to-digital converter, and an optimized analog front-end resulted in a highly efficient, compact, and real-time depth sensing platform, ready for a final engineering step. The results obtained represent a feasibility study for a potential commercial product, that is low-cost and small-size, with different consumer applications.

Section: RESEARCH PAPER

Keywords: 3D camera; LiDAR; MEMS mirrors; rangefinder; optical scanning

Citation: P. Diotti, D. Caltabiano, A. A. Pomarico, G. Roselli, M. Norgia, Development of a real-time 3D camera based on micro-electromechanical systems mirrors, Acta IMEKO, vol. 15 (2026) no. 1, pp. 1-8. DOI: 10.21014/actaimeko.v15i1.2252

Section Editor: Francesco Lamonaca, University of Calabria, Italy

Received November 27, 2025; **In final form** February 12, 2026; **Published** March 2026

Corresponding author: Michele Norgia, e-mail: michele.norgia@polimi.it

1. INTRODUCTION

LiDAR (Light Detection and Ranging) technology has become indispensable across various sectors, including autonomous vehicles, industrial automation, and environmental monitoring. By emitting laser pulses and measuring the time it takes for reflections to return, LiDAR systems construct precise 3D representations of environments [1]. The accuracy and efficiency of these systems heavily depend on the underlying time-of-flight (ToF) methodologies employed, as each approach (e.g., direct vs. indirect) entails specific trade-offs in measurement range, resolution, and speed that ultimately shape LiDAR system performance [2]. Different ToF technologies have been developed in recent times. The common principle of such technologies exploits the relation between the time it takes for a wave of light to travel from a source to an object and back, and the distance travelled.

There are two main families of ToF methods. dToF (direct time-of-flight) involves a direct measurement of the time until reflection is detected. Direct ToF systems send out short light pulses and then measure the time it takes for some of the emitted light to come back, generally using SPAD (single-photon avalanche diode)-based detectors [3].

iToF (indirect time-of-flight) systems send out continuous, intensity modulated light and measure the phase shift between the transmitted waveform and received waveform. This phase shift is proportional to the distance of the reflecting object.

ToF technologies find one of their main applications in the LiDAR devices. LiDAR is a method for determining ranges by targeting a scene with a laser source (transmitter) and measuring the time for the reflected light to return to the receiver. In particular, in scanning LiDAR, the transmitter is a scanning, narrow emitter beam which is being moved across the field of view (FoV) over time; a mechanical solution or micro-mirrors are used for beam steering. LiDAR readings can then be used to form 'point clouds', which in turn allow to create three-dimensional models of objects or topographical maps of whole areas.

Traditional LiDAR systems often rely on mechanical components for beam steering, which can be bulky and prone to wear [4], [5]. In contrast, MEMS (micro-electromechanical system) mirrors are a compact and reliable alternative for directing laser beams across the desired field of view, because

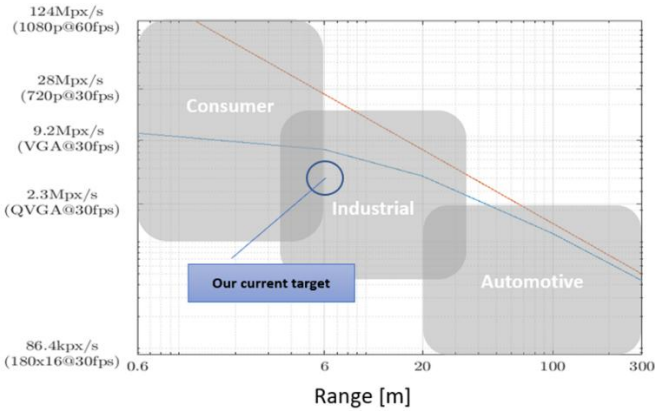

Figure 1. Typical performances required by 3D measurement systems for different applications: image resolution vs. distance range. The proposed project has a target between consumer and industrial application, with a desired image resolution QVGA and a measurement range of a few meters.

they have fewer moving parts, reducing mechanical fatigue and increasing overall durability, while maintaining high precision in beam steering. The integration of MEMS technology not only reduces the system's size and weight but also enhances its robustness and scanning speed [6].

However, MEMS-based LiDAR systems face several challenges:

- Accuracy limitations: the small size of MEMS mirrors can lead to limited aperture, affecting the system's ability to collect reflected light efficiently, which may reduce accuracy [4]. For example, in table 1 of [7], a comparison is reported between different realizations of MEMS-based LiDAR, showing a standard deviation in the order of 5–10 cm over a range of a few meters (1–2 % of the full range) with the same order of magnitude of non-linearity.
- Scanning efficiency: achieving a wide field of view while maintaining high resolution requires precise control of MEMS mirrors. The trade-off between scan speed and resolution necessitates sophisticated control algorithms [6].
- Integration with FPGA processing: implementing real-time signal processing for high-frequency data on FPGAs demands careful design to avoid bottlenecks and ensure low-latency performance [8].

In this study, we introduce a dToF-based scanning LiDAR prototype that leverages MEMS mirrors for agile beam steering and an FPGA-based processing unit for real-time 3D image reconstruction. The specifications could target both industrial and consumer applications, as illustrated in Figure 1: the target operating distance is up to a few meters, with an image resolution QVGA (quarter video graphics array), corresponding to 320 × 240 pixels. The proposed approach is still at the feasibility study stage, but it is already organized in such a way as to be able to lead to the creation of extremely compact instruments (just a few millimetres in size), at a potentially very low cost for large production volumes.

The structure of this paper is as follows: Section 2 recalls briefly the state of the art in optical distance measurement sensors. Section 3 delves into the system architecture and implementation details, covering the optomechanical components, FPGA-based processing framework, and analogue signal handling. Section 4 discusses the experimental setup and presents the results from various validation tests. Section 5 offers a performance analysis, comparing our system with existing solutions. Finally, Section 6 concludes the paper, summarizing our findings and suggesting directions for future research.

2. STATE OF THE ART

For the application to 3D metrology, different optical techniques are available for distance measurement [2], and different beam steering technologies can be used for laser scanning [4].

2.1. Optical rangefinders

Optical triangulation is a widely used technique for measuring distances based on geometric principles. A laser source emits a beam toward a target, and the reflected light is captured by a detector positioned at a known baseline distance. By determining the angle at which the reflected light returns, the system can calculate the distance between the sensor and the object with high accuracy [9]. This method is particularly advantageous for short-range applications due to its ability to achieve micrometre-level precision. However, the effectiveness of triangulation diminishes over long distances due to geometric constraints, making it unsuitable for large-scale LiDAR mapping. It is commonly employed in industrial metrology, robotic vision, and precision manufacturing, where high accuracy is required at relatively short distances [10].

Interferometric techniques allow to measure a target distance, typically by modulating the wavelength of a laser beam and measuring the frequency of the interferometric signal, proportional to the target distance [11]. Normally these kinds of instruments are quite complex, high-cost, and cannot reach a high repetition rate. Among the interference techniques, a simpler approach based on retroreflection stands out: self-mixing interferometry leverages the interference occurring within the laser cavity when the emitted and backscattered light interact. Using this technique, it is possible to create distance meters with sub-millimetre accuracy for distances of up to a few meters [12]. However, the repetition rate is limited to a few kHz.

Time-of-flight (ToF) techniques determine the distance between the sensor and the target by measuring the time taken for a laser pulse to travel to the object and back. By utilizing the known speed of light, the distance can be accurately calculated [2]. This method is further divided into direct and indirect approaches. Direct time-of-flight relies on fast photodetectors to measure the exact travel time of laser pulses, making it suitable for applications requiring long-range measurements. Indirect time-of-flight, on the other hand, measures the phase shift between emitted and received signals, offering improved accuracy for shorter ranges, but slower repetition rate. ToF technology is commonly employed in autonomous vehicles, airborne LiDAR, and geospatial mapping, as it provides a balance between range, accuracy, and cost effectiveness [1].

Frequency modulated continuous wave (FMCW) LiDAR is an advanced technique that modulates the laser frequency over time and analyses the beat frequency of the returned signal [13]. This approach allows for simultaneous range and velocity measurements with high precision. FMCW LiDAR is known for its immunity to ambient light interference, making it highly reliable even in challenging environmental conditions. Additionally, its range can exceed 300 meters, making it particularly suitable for applications such as automotive LiDAR, defence, and remote sensing. This technique is expected to play a crucial role in the future development of high-performance LiDAR systems due to its superior resolution and accuracy.

2.2. Laser beam steering technologies

Rotating mirrors represent one of the earliest and most widely used methods for laser beam steering. A motorized mirror deflects the laser beam across a predefined field of view, allowing for the systematic scanning of the surrounding environment. This technique provides high accuracy but is inherently limited by mechanical inertia, which constrains scanning speed. Furthermore, rotating mirrors can be susceptible to vibrations, potentially impacting measurement precision. Despite these drawbacks, they remain a preferred solution in traditional LiDAR systems and airborne applications where robustness and reliability are critical [4]. Another widely employed mechanical solution is the galvanometer, which is used to move the mirrors [14].

Risley prisms utilize two rotating wedge-shaped prisms to control beam direction through controlled refraction [15]. This technique offers a wide field of view without relying on mechanical components that are prone to wear and tear. The ability to precisely direct the laser beam without significant mechanical constraints makes Risley prism-based scanning systems highly suitable for spaceborne and defence applications, where reliability and longevity are essential.

A more recent solution is based on MEMS technology that employs miniature mirrors actuated by microfabricated structures, to control laser beam deflection [6]. This method enables rapid scanning with relatively high precision while reducing the overall size of the LiDAR system. MEMS-based scanning systems are widely adopted in compact, solid-state LiDAR designs, particularly in the automotive industry [7], [16], [17]. By eliminating the need for bulky mechanical components, MEMS technology contributes to the development of lightweight, cost-effective, and energy-efficient LiDAR solutions.

Optical phased arrays (OPA) represent a cutting-edge approach to beam steering that eliminates the need for moving parts. Instead of relying on mechanical motion, OPA systems utilize phase-controlled laser emitters to manipulate the direction of the emitted beam through interference [18]. This enables ultra-fast electronic scanning with extremely high accuracy. Due to their solid-state nature, optical phased arrays are highly durable and resistant to mechanical failures. They are particularly promising for next-generation LiDAR applications, including military surveillance and high-performance autonomous navigation.

3. SYSTEM ARCHITECTURE & IMPLEMENTATION

This section delineates the comprehensive architecture and implementation of our MEMS-based scanning LiDAR prototype, emphasizing its optomechanical design, FPGA-based digital processing, and analogue front-end signal conditioning.

The proposed LiDAR system is meticulously engineered to achieve precise 3D environmental mapping while maintaining a compact footprint. It is designed to operate within a range of up to 1 meter with a spatial resolution of 400 × 300 pixels, ensuring high accuracy and detail in environmental reconstruction. The block diagram of the LiDAR system is shown in Figure 2, reporting the main connections between four primary sub-systems:

1) The information processing and system command module, where we use an FPGA to manage all the system. It regulates the laser command system, drives mirror controllers, processes incoming information (measures ToF), and manages communication to a personal computer and a display.

2) The laser driver and micromirror module: the system includes a single, fixed laser the firing window of which is defined by the movement of two ST micromirrors that allow the laser to change the firing point to create a 24° × 17° acquisition window for a total of 400 × 300 pixels. By varying the micromirror command signals, we can define a specific trajectory for covering the entire field of view.

3) The analogue interface module: its task starts from the reception of the light signal reflected from the target, through a photodetector (specifically an MPPC, multi-pixel photon counter), and its processing and conversion into a signal accessible by the receiving FPGA. After the laser pulse hits the target and returns, it is processed and made available to the FPGA through an analogue front-end.

4) The display module: the signal reconstructed by the FPGA is displayed on the screen through an HDMI interface and can be modified in real time through a user interface, which is controllable via a HDMI port through a dedicated graphical user interface (GUI).

This modular configuration ensures flexibility and scalability, rendering the system suitable for diverse applications, such as autonomous navigation, industrial monitoring, and augmented reality.

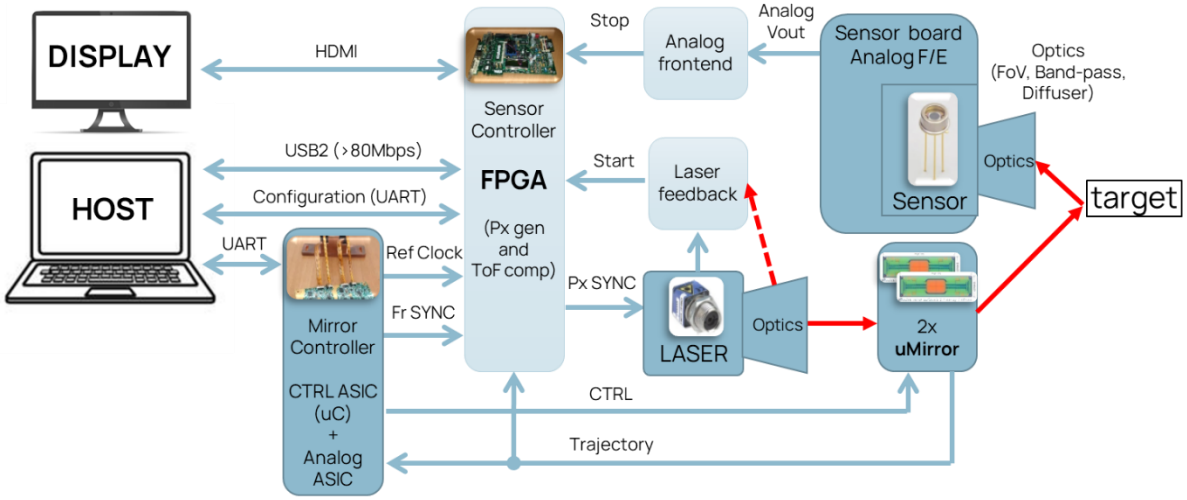

Figure 2. 3D camera project block diagram: the FPGA regulates the laser command system, drives mirror controllers, processes incoming information (measures ToF), and manages communication to the outside (with a PC for configuration and debug, and with a display for 3D image output via HDMI).

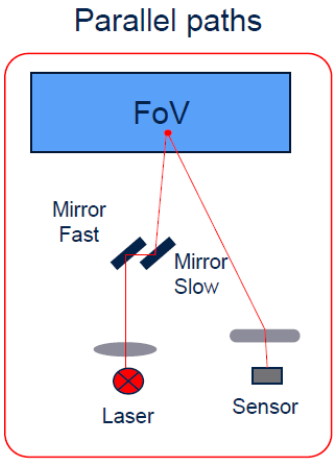

Figure 3. LiDAR block diagram, with separated transmission and detection path: MEMS mirrors act only on the emitted laser light; the detector has separate optics.

3.1. Optomechanical system

The LiDAR initially employs a pulsed laser diode operating at a wavelength of 640 nm, selected in the first prototype to simplify alignment, thanks to its visibility. The laser emits pulses with an 8 ns duration and a repetition rate of 8 MHz, with a peak power of about 100 mW.

Beam steering is achieved through the integration of two MEMS scanning mirrors, by STMicroelectronics [19]. In order to have low power consumption, we decided to let the horizontal mirror move at a resonant frequency of about 27.5 kHz with a maximum opening angle of 14 degrees. The vertical mirror moves in a linear way, covering about 8° of the field of view. The synergistic operation of these mirrors facilitates a comprehensive acquisition window of 24° × 17°, achieving a resolution of 400 × 300 pixels.

The receiver subsystem is designed in parallel, as shown in Figure 3, in order to take advantage of a bigger lens for improving the received signal. It incorporates a multi-pixel photon counter (MPPC) as the photodetector, renowned for its high sensitivity and low noise characteristics [20]. To mitigate ambient light interference, bandpass optical filters are employed, ensuring that only the desired wavelength is detected. This design enhances the signal-to-noise ratio (SNR), which is critical for accurate distance measurements [21].

3.2. FPGA-based digital processing

The time-to-digital converter (TDC), implemented on a Xilinx Virtex-7 FPGA, is central to the system's digital processing. This choice is driven by the FPGA's high-speed logic capabilities and adaptable architecture. The TDC is responsible for calculating the time-of-flight by capturing the 'Start' signal, corresponding to the laser pulse emission, and the 'Stop' signal, representing the reflected pulse detected by the MPPC sensor. Operating with a resolution of 208.33 picoseconds, achieved through a 400 MHz clock with a six-phase delay method, the system effectively simulates a 4.8 GHz sampling rate. This precision translates to a distance measurement resolution of approximately 3 cm.

The FPGA also orchestrates the synchronization of MEMS mirror movements, generating real-time control waveforms matching the mirrors' resonant and non-resonant drive signals. This ensures that each laser pulse is triggered in tandem with the mirror positions, aligning the pulse trajectory precisely with the corresponding pixel location in the reconstructed 3D image. The control algorithms support various scanning patterns, including Lissajous figures, linear sweeps, and sawtooth waveforms, allowing for adaptive acquisition strategies tailored to specific application requirements.

Processed 3D depth maps are rendered in real time via an HDMI interface, providing immediate visual feedback. Additionally, system control and parameter adjustments are facilitated through a UART-connected graphical user interface (GUI). The FPGA architecture is designed to handle high data throughput efficiently, ensuring low-latency performance, which is essential for dynamic environments.

3.3. Analog front-end and signal conditioning

The task of the electronic interface is to create a link between the photodetector and the FPGA, with the aim of processing the received signal and allowing the board to receive the correct information. The analogue front-end starts with the MPPC photodetector, which converts incident photons into an electrical current. This current is then transformed into a voltage signal by a transimpedance amplifier (TIA), optimized for low noise and high bandwidth to accurately capture the rapid transients of the reflected laser pulses.

At the output of this block, we have a voltage pulse. However, this signal cannot be used for our application since it is not a digital signal, and therefore the FPGA struggles to process it correctly. The simplest solution would be to introduce a comparator with a threshold into the system. In this case, the system would actually generate a digital signal at the output, but it is subject to an error. In fact, as the intensity of the light received by the sensor varies, the amplitude of the pulse generated by the charge amplifier also varies, and this dependence means that the signal can reach the threshold at different times. For a correct processing of information by the FPGA, we will need the time interval between the laser pulse emission and its reception to be immune to this type of error.

To address timing inaccuracies caused by variations in signal amplitude, a constant fraction discriminator (CFD) has been implemented. The central idea of the CFD is to create a delayed and an attenuated version of the received signal. The timing point at the intersection of the attenuated input signal and the delayed input signal does not depend on the signal amplitude. In this way, the CFD can assign the timing point on a constant fraction of the input signal, making the timing point insensitive to the amplitude of the pulse received by the sensor [22]. This technique allows to maintain measurement accuracy across a range of signal intensities and distances. Figure 4 shows the block diagram of the analogue front-end implemented in a PCB board. The first block is an amplifier, which is necessary because the photo-detected signal on a white target has a maximum peak

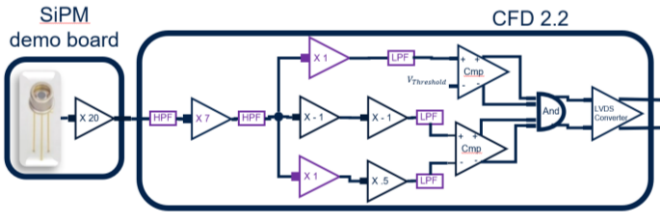

Figure 4. Block diagram of the analogue front-end with constant fraction discriminator: the signal delayed is compared with the signal attenuated. The crossing instant does not depend on the signal amplitude. The upper comparator is introduced to avoid false counts when the pulse amplitude is too low.

amplitude of 120 mV at close distances and decreases to about 10 mV if the target is 1 m away. In the next block, we will implement the mathematical algorithm underlying the CFD, so we created one analogue chain to set a variable delay to the input signal, and another chain with a fixed attenuation. The delay chain is realized by the cascade of two all-pass filters.

By varying the values of passive components, we can act on the delay value with respect to the input signal. The delayed and the attenuated signals are the input of a comparator that snaps in correspondence of the intersection point [22]. Due to the presence of noise, we had to introduce an additional enable chain, which allows the output only when the signal amplitude is high enough, in order to avoid spurious counting.

3.4. Graphic interface

The reconstructed image is displayed through an HDMI interface, but our system has a second communication with the UART port for managing and controlling the 3D camera.

This communication is implemented through a graphic interface, shown in Figure 5, that allows us to display the image directly from the PC without going through the HDMI output (with a reduced frame rate of 1 image per second due to the limitation of the UART port). It also allows to save the image shown in both PNG and text format. Through the text file, we can read and see all the values of the 400 × 300 matrix that the image is composed of, in this way we can test the proper working and calibrate the system.

The interface allows to modify the colour scale with which the image is displayed on the HDMI screen and therefore change the tones of the image itself. It also directly displays some statistics on the screen, such as the average distance of the pixels during the frame under examination, the number of pixels in time-out (for which no response has been received, therefore the maximum value has been assigned), or the points where the laser did not pass (in case of errors due to the laser trajectory algorithm).

In summary, the integration of advanced optomechanical components with sophisticated FPGA-based processing and a robust analogue front-end design culminates in a high-performance MEMS-based LiDAR system.

4. MEASUREMENT RESULTS

The subsequent sections will delve into the experimental validation and performance metrics that underscore the efficacy of this approach.

4.1. Simulation studies

Prior to hardware implementation, extensive MATLAB simulations were conducted to model and optimize the laser scanning trajectories facilitated by the MEMS mirrors. The primary goal of these simulations was to predict the FoV coverage and ensure uniform spatial point distribution. Various scanning patterns, including Lissajous, sawtooth, and linear sweeps, were tested to identify the most effective approach for maximizing spatial resolution while minimizing overlap and voids. The results from these simulations provided crucial insights into optimizing mirror control algorithms and ensuring efficient environmental mapping. Additionally, Vivado simulations were employed to validate the implementation of the TDC within the FPGA framework, ensuring precise signal acquisition and processing at a resolution of 208.33 picoseconds.

4.2. Hardware testing

The analogue front-end, responsible for signal amplification and conditioning, underwent rigorous testing, using both LED and laser sources. Initial tests using a red LED, with an aligned mirror as the target, served as a controlled benchmark to evaluate the system's baseline performance. These tests revealed a measurement accuracy of 40 mm over a range of 1.4 meters, in good coherence with the TDC resolution of about 33 mm. Subsequently, tests were conducted with a 640 nm laser source on a non-cooperative target, to simulate real-world conditions. The achieved accuracy was about 60 mm, across distances ranging from 20 cm to 1.1 m, mainly limited by the low SNR, due to the limited peak power of the red laser used in this feasibility demonstrator. One of the characterization campaigns is shown in Figure 6: the measurement was repeated on a white paper target, positioned from 30 cm to 140 cm, with 10 cm steps. For each distance, 60,000 measurements were acquired, reported as the probability density function in Figure 6 (note that the value is intentionally not normalized, and the absolute numbers of

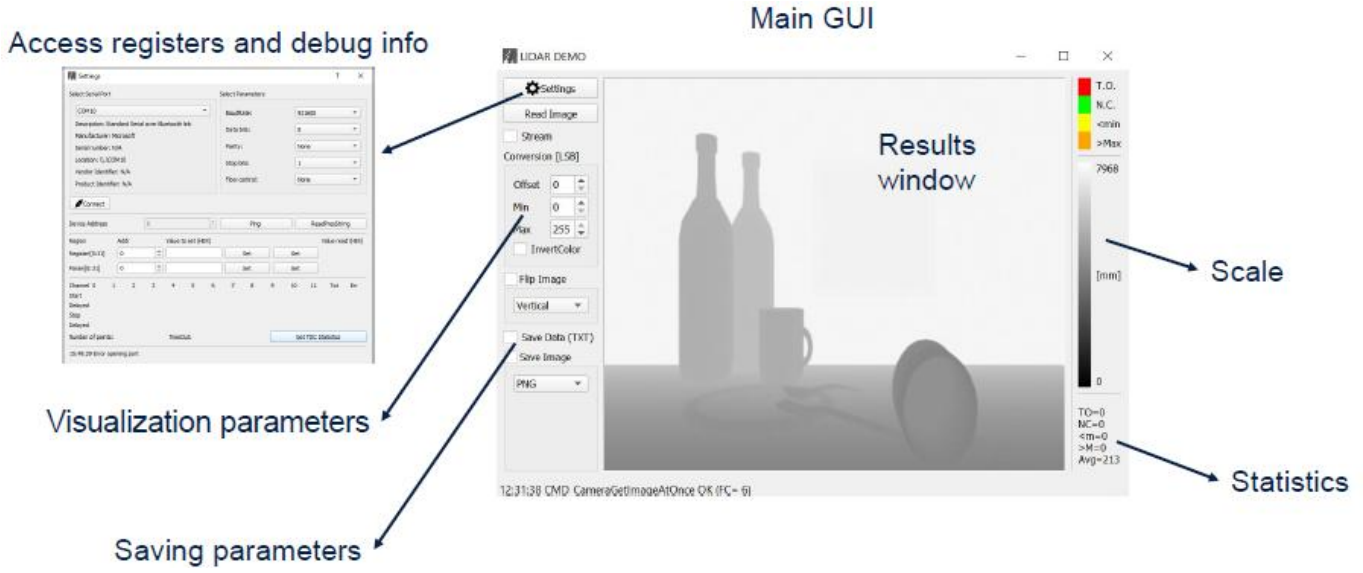

Figure 5. Graphic interface implemented on a personal computer: it allows to set and control the HDMI output and access registers and debug info to verify the correct working of the system, while showing the acquired 3D image with a frame rate limited to 1 image per second.

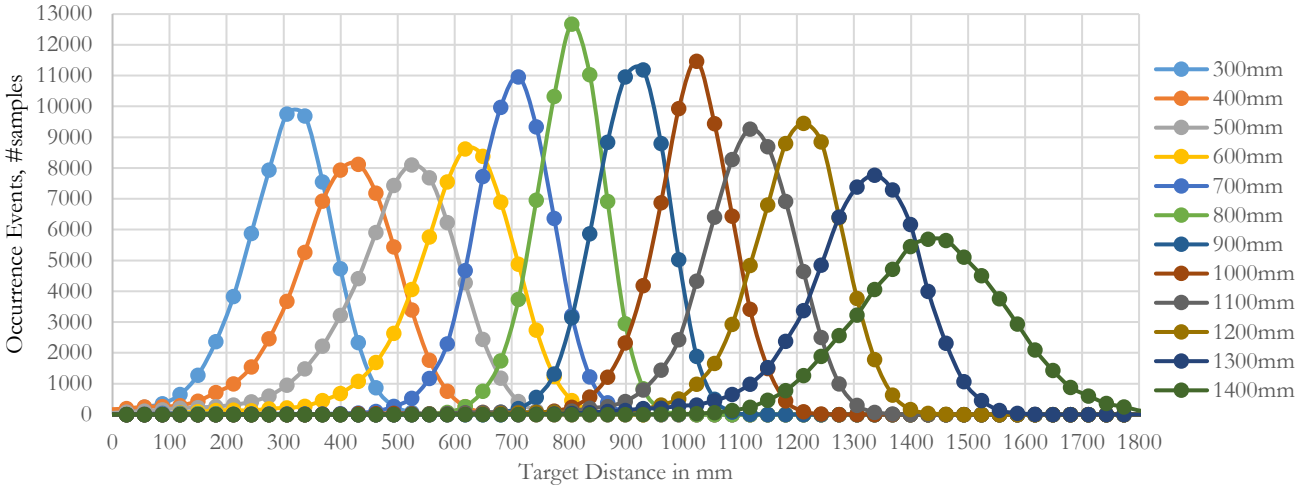

Figure 6. LiDAR characterization as a function of target distance. The probability density function (not normalized) is taken over 60,000 measurements for each distance.

measurements corresponding to each distance are reported). The graphs clearly show the quantization of approximately 33 mm (dots), due to the TDC resolution, which, however, does not significantly limit the measurement accuracy.

These evaluations confirmed that the front-end maintained signal integrity under varying illumination conditions and provided a robust foundation for accurate time-of-flight calculations.

Following the validation of individual subsystems, the fully integrated LiDAR prototype was tested in a controlled environment using a flat white target. The system successfully achieved an FoV of 24° × 17° with a resolution of 400 × 300 pixels. The MEMS mirrors work in a synchronized manner, executing predefined scanning patterns with high precision. The resultant point cloud data provided a highly accurate representation of the target's spatial features, demonstrating the system's capability for real-time 3D reconstruction.

4.3. 3D object scanning and post-processing

To assess the system's performance in a practical scenario, 3D scans of a complex object—a white teddy bear—were conducted. The system effectively captured the depth variations of the object, with distances ranging from 470 mm (proximal features) to 800 mm (background). The real-time depth maps, displayed via a graphical user interface, utilized a colour gradient to represent depth variations, enhancing the interpretability of spatial data.

Post-processing techniques were applied to further refine the depth data. Frame averaging over 30 frames significantly reduced depth fluctuations, leading to smoother and more precise depth representations. Extending the averaging to 100 frames provided marginal improvements, demonstrating a trade-off between processing time and accuracy enhancement. The optimal choice of 33 frames per second was determined as a balance between computational efficiency and measurement fidelity.

Figure 7 shows an example of a real measurement, both in false colours and in 3D. For the tests, we used a white teddy bear, positioned in the centre of the field of view, against a white flat background. The teddy bear has a depth (along the optical axis of the LiDAR system) of about 10 cm, and its distance from the LiDAR ranges from 47 cm to 57 cm, while the distance of the white background is 80 cm.

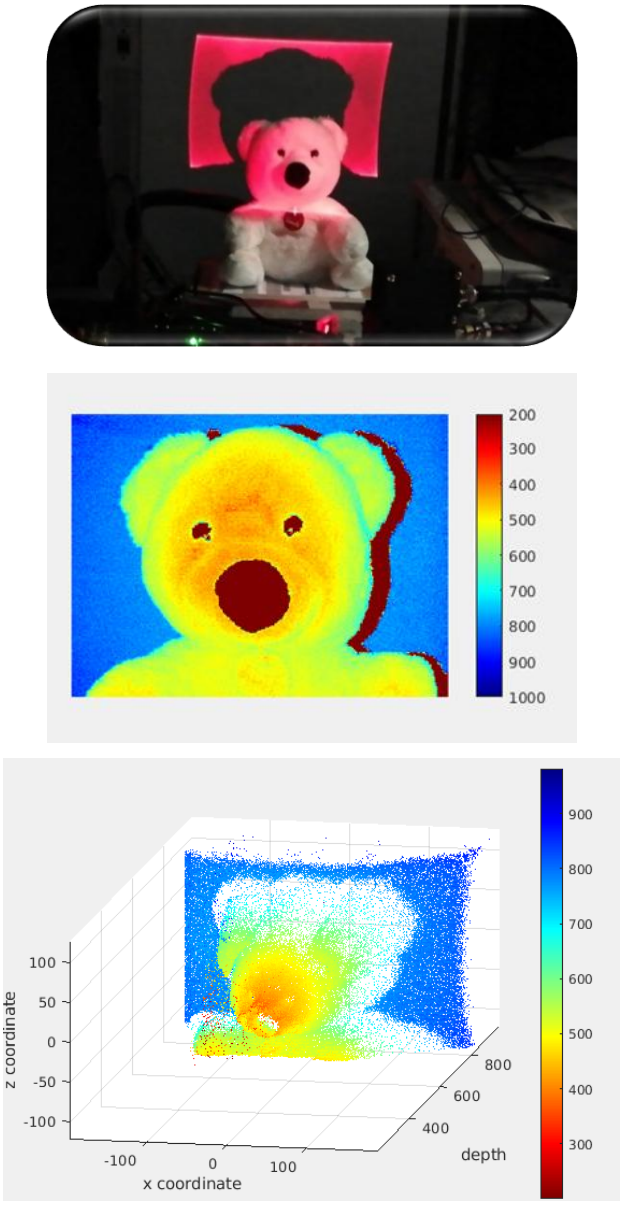

Figure 7. Example of 3D real-time measurement results, taken on a teddy bear.

5. DISCUSSION AND CONCLUSION

In the realm of LiDAR technology, the integration of MEMS has emerged as a transformative approach, offering a balance between performance and compactness. This section delves into a comprehensive analysis of the developed MEMS-based LiDAR system, juxtaposing its performance against existing technologies, discussing inherent limitations, and proposing avenues for future enhancements.

5.1. Performance analysis

The experimental validation of the MEMS-based LiDAR system underscores its capability to deliver high-resolution three-dimensional imaging with real-time data processing. Key performance metrics, such as depth accuracy, FoV, and spatial resolution, have been meticulously evaluated to ensure alignment with the intended application requirements.

The system consistently achieves a depth accuracy of 60 mm, within a measurement range spanning from 20 cm to about 1 m. This precision is facilitated by the TDC integrated within the FPGA architecture, which boasts a resolution of 208.33 picoseconds, correlating to a distance measurement precision of approximately 33 mm.

The LiDAR system offers an FoV of 24° × 17°, coupled with a spatial resolution of 400 × 300 pixels. This configuration ensures comprehensive environmental mapping, capturing intricate details essential for accurate object detection and scene reconstruction. The utilization of MEMS mirrors facilitates agile beam steering, enabling the system to cover the designated FoV efficiently. A notable attribute of the system is its proficiency in real-time data acquisition and processing. The FPGA-based architecture, in conjunction with optimized control algorithms, allows for rapid signal processing, thereby minimizing latency.

In comparative analyses, the proposed MEMS-based LiDAR demonstrated performance metrics comparable with existing commercial systems [23]–[25]. Note that the actual prototype is extremely limited by the company's decision to build a feasibility demonstrator with a visible laser source and limited power. An engineered version of the optical component would certainly lead to higher accuracy, but the entire architecture already provides the basis for subsequent commercial development. The system's compact design and real-time processing capabilities offer advantages in scenarios where size and speed are critical. These attributes position the prototype as a viable candidate for integration into platforms requiring efficient and accurate environmental sensing.

5.2. Final remarks

This study has successfully demonstrated the feasibility of a MEMS-based scanning LiDAR system that is compact, efficient, and capable of high-resolution 3D depth sensing. Through extensive experimental validation, we have confirmed that the system meets the performance requirements for short-range, real-time depth imaging applications. The integration of meticulous simulations, hardware testing, and effective post-processing techniques has culminated in a robust system poised for deployment in a wide range of applications, which include enhancing obstacle detection and environment mapping in autonomous mobile robots and industrial robotic arms; integrating it into advanced driver assistance systems (ADAS) for collision avoidance and parking assistance in next-generation vehicles; industrial automation and smart manufacturing, that is, enabling real-time depth perception for machine vision systems, improving quality control and robotic assembly precision.

REFERENCES

[1] S. Royo, M. Ballesta-Garcia, An Overview of Lidar Imaging Systems for Autonomous Vehicles, Appl. Sci. 9 (2019) 19, p. 4093. DOI: 10.3390/app9194093

[2] M. Amann, T. Bosch, M. Lescure, R. Myllylä, M. Rioux, Laser ranging: a critical review of unusual techniques for distance measurement, Opt. Eng. 40 (2001) 1, pp. 10–19. DOI:10.1117/1.1330700

[3] S. Cova, M. Ghioni, A. Lotito, I. Rech, F. Zappa, Evolution and Prospects for Single-Photon Avalanche Diodes and Quenching Circuits, Journal of Modern Optics 51 (2004) 9–10, pp. 1267–1288. DOI: 10.1080/09500340408235272

[4] T. Raj, F. H. Hashim, A. B. Huddin, M. F. Ibrahim, A. Hussain, A Survey on LiDAR Scanning Mechanisms, Electronics 9 (2020) 5, p. 741. DOI: 10.3390/electronics9050741

[5] C. Zuo, Y. He, 2D FPCB micromirror for scanning LIDAR, Journal of Micromechanics and Microengineering 33 (2022) 12, p. 125001. DOI:10.1088/1361-6439/ac9e62

[6] D. Wang, C. Watkins, H. Xie, MEMS Mirrors for LiDAR: A Review, Micromachines 11 (2020) 5, p. 456. DOI: 10.3390/mi11050456

[7] C. Niclass, K. Ito, M. Soga, H. Matsubara, I. Aoyagi, S. Kato, M. Kagami, Design and characterization of a 256x64-pixel single-photon imager in CMOS for a MEMS-based laser scanning time-of-flight sensor, Opt. Exp. 20 (2012) 11, pp. 11863–11881. DOI: 10.1364/OE.20.011863

[8] C. González, M. Ruiz, A. Carpeño, A. Piñas, D. Cano-Ott, J. Plaza, T. Martinez, D. Villamarin, Hardware Acceleration of Digital Pulse Shape Analysis Using FPGAs, Sensors 24 (2024) 9, p. 2724. DOI: 10.3390/s24092724

[9] F. J. Pipitone, T. G. Marshall, A wide-field scanning triangulation rangefinder for machine vision, Int. J. Robot. Res. 2 (1983) 1, pp. 39–49. DOI: 10.1177/027836498300200104

[10] M. Norgia, M. Annoni, A. Pesatori, C. Svelto, Dedicated Optical Instruments for Ultrasonic Welder Inspection and Control, Measurement 43 (2010) 1, pp. 39–45. DOI: 10.1016/j.measurement.2009.06.006

[11] F. Cavedo, P. Esmaili, M. Norgia, Self-Mixing Laser Distance-Sensor Enhanced by Multiple Modulation Waveforms, Sensors 22 (2022) 21, p.8456. DOI: 10.3390/s22218456

[12] F. Cavedo, P. Esmaili, M. Norgia, Study of the Errors in Interpolated Fast Fourier Transform for Interferometric Applications, Metrology 4 (2024) 1, pp. 117–130. DOI: 10.3390/metrology4010008

[13] J. Lee, J. Hong, K. Park, Frequency Modulation Control of an FMCW LiDAR Using a Frequency-to-Voltage Converter, Sensors 23 (2023) 10, p. 4981. DOI: 10.3390/s23104981

[14] T. Hegna, H. Pettersson, K. Laundal, K. Grujic, 3D laser scanner system based on a galvanometer scan head for high temperature applications, Proc. of SPIE, Munich, Germany, 23–26 May 2011, no. 8082. DOI:10.1117/12.888985

[15] Y. Zhou, Y. Lu, M. Hei, G. Liu, D. Fan, Motion control of the wedge prisms in Risley-prism-based beam steering system for precise target tracking, Appl. Opt. 52 (2013) 12, pp. 2849–2857. DOI:10.1364/AO.52.002849

[16] B. L. Stann, J. F. Dammann, M. M. Giza, W. B. Lawler, H. M. Nguyen, L. C. Sadler, MEMS-scanned ladar sensor for small ground robots, Proc. of SPIE, 2010, no. 7684, pp. 76841E-1–76841E-12. DOI: 10.1117/12.850388

[17] I. Aoyagi, K. Shimaoka, S. Kato, W. Makishi, Y. Kawai, S. Tanaka, T. Ono, M. Esashi, K. Hane, 2-Axis MEMS scanner for a laser

range finder, Proc. IEEE Int. Conf. Opt. MEMS Nanophoton., Istanbul, Turkey, 2011, pp. 39–40.
DOI: 10.1109/OMEMS.2011.6031035

[18] Y. Yi, D. Wu, V. Kakdarvishi, B. Yu, Y. Zhuang, A. Khalilian, Photonic Integrated Circuits for an Optical Phased Array, Photonics 11 (2024) 3, pp. 243.
DOI: 10.3390/photonics11030243

[19] P. Frigerio, R. Tarsi, L. Molinari, G. Maiocchi, A. Barbieri, G. Langfelder, A novel closed-loop architecture for accurate micromirror trajectory control in linear scanning MEMS-based projectors, Proc. of SPIE 11697, MOEMS and Miniaturized Systems XX, Online, 6–12 March 2021, 1169706.
DOI: 10.1117/12.2577186

[20] K. Yamamoto, K. Yamamura, K. Sato, T. Ota, H. Suzuki, S. Ohsuka, Development of Multi-Pixel Photon Counter (MPPC), Proc. of 2006 IEEE Nuclear Science Symposium, San Diego, USA, 29 October–01 November 2006, pp. 1094–1097.
DOI: 10.1109/NSSMIC.2006.356038

[21] J. Illade-Quinteiro, V. M. Brea, P. Lopez, D. Cabello, G. Doménech-Asensi, Ginés, Distance Measurement Error in Time-of-Flight Sensors Due to Shot Noise, Sensors, 15 (2015) 3, pp. 4624–4642.
DOI: 10.3390/s150304624

[22] R. Zheng, G. Wu, The Constant Fraction Discriminator in Pulsed Time-of-Flight Laser Rangefinding, Frontiers of Optoelectronics 5 (2012), pp. 182–186.
DOI: 10.1007/s12200-012-0229-2

[23] B. Behroozpour, P. A. M. Sandborn, M. Wu, B. Boser, Lidar System Architectures and Circuits, IEEE Comm. Mag. 55 (2017), pp. 135–14.
DOI: 10.1109/MCOM.2017.1700030

[24] C. Niclass, M. Soga, E. Charbon, 3D imaging based on single-photon detectors, 2nd Symposium on Range Imaging (RIM'07), Zurich, Switzerland, 2007, pp. 34–41. Online [Accessed 16 March 2026]
https://infoscience.epfl.ch/handle/20.500.14299/26378

[25] C. Niclass, A. Rochas, P.-A. Besse, E. Charbon, Design and characterization of a CMOS 3-D image sensor based on single photon avalanche diodes, IEEE J. Solid-State Circuits 40 (2005) 9, pp. 1847–1854.
DOI: 10.1109/JSSC.2005.848173